

# Perception-based multiplicative noise removal using SDEs

An Vuong  
Oregon State University  
Corvallis, OR, 97331  
vuonga2@oregonstate.edu

Thinh Nguyen  
Oregon State University  
Corvallis, OR, 97331  
thinhq@oregonstate.edu

## Abstract

*Multiplicative noise, also known as speckle or pepper noise, commonly affects images produced by synthetic aperture radar (SAR), lasers, or optical lenses. Unlike additive noise, which typically arises from thermal processes or external factors, multiplicative noise is inherent to the system, originating from the fluctuation in diffuse reflections. These fluctuations result in multiple copies of the same signal with varying magnitudes being combined. Consequently, despeckling, or removing multiplicative noise, necessitates different techniques compared to those used for additive noise removal.*

*In this paper, we propose a novel approach using Stochastic Differential Equations based diffusion models to address multiplicative noise. We demonstrate that multiplicative noise can be effectively modeled as a Geometric Brownian Motion process in the logarithmic domain. Utilizing the Fokker-Planck equation, we derive the corresponding reverse process for image denoising. To validate our method, we conduct extensive experiments on two different datasets, comparing our approach to both classical signal processing techniques and contemporary CNN-based noise removal models. Our results indicate that the proposed method significantly outperforms existing methods on perception-based metrics such as FID and LPIPS, while maintaining competitive performance on traditional metrics like PSNR and SSIM.*

## 1. Introduction

Multiplicative noise removal is a long standing problem in computer vision and has been studied by many researchers over the past few decades [1][2][3][4][5]. Unlike additive noise, which is usually the result of thermal fluctuations during image acquisition or transmission, multiplicative noise happens when multiple copies of the signal with random scaling factors are added together. This often happens due to the internal physical construction of the image capturing devices, i.e. optical lenses, radar/laser imaging,



Figure 1. Samples generated by our methods, on images randomly selected from CelebA dataset. From left to right are the original, corrupted by multiplicative noise (noise level 0.08), and denoised versions.

ultrasound sensors, etc. Because of this, removing multiplicative noise, sometimes referred to as despeckling, often requires more sophisticated approaches compared to its counterpart additive noise. Popular approaches include modelling the noise using Partial Differential Equations (PDEs) [6] [7], converting into additive domain and optimize using Total Variation (TV) objective [8], and applying MAP estimation [9]. Classical methods based on block-matching technique also works decently for this problem [10]. More recently, deep learning based methods have been introduced with great successes in denoising performance [11][12][13]. These methods usually use image-to-image translation architecture, where the neural networks directly predict the clean images, or the amount of noise generated

by the stochastic process, without much assumption on the noise dynamics. Thus, many of these models can be applied to reverse different kinds of corruptions, including multiplicative noise. However, these techniques mostly rely on "per-pixel" metrics such as MSE, PSNR, or SSIM, which has been observed to not correlate well with human perception [14].

In this work, we propose the novel application of Stochastic Differential Equations (SDEs) to perform multiplicative noise removal. We show that the dynamics of multiplicative noise is well captured by SDEs, specifically Geometric Brownian motion. We then derive the reverse SDEs which are used to generate denoised samples. By running extensive experiments on two different datasets, we demonstrate the effectiveness of our method on creating clean images that achieve high perception scores. We detail the construction of our approach in Section 3.

## 2. Related works

Over the last few years, with the advances of deep learning, there has been active research in applying CNN to image denoising problems, especially for speckle or multiplicative noise. Notable works can be found in [15][16][17]. In these texts, the common theme is to perform image-to-image translation with a Convolutional neural network (CNN) acting as the mapping function. This CNN is usually trained to minimize MSE or PSNR loss directly on the pairs of clean and noisy images. Some works propose to use specially-crafted features as the input, such as frequency features [18], or wavelet features [19], and sub-bands [20]. These works are usually limited to grayscale images, and are often matched in performance by DnCNN[11], and can be beaten by NAFNet[13], MPRNet[21], or Restormer[22].

Recently, there is a line of works applying diffusion technique to this problem. In [23], the authors propose a DDPM-like architecture for despeckling, but this model needs to be re-trained for each noise level. Similarly, [24][25] also use DDPM framework with minor modifications. These works still limit their testing to grayscale images only. We find the discussion in [26] to be the most related to our work, albeit with different assumption of the noise characteristics and the construction of the diffusion process, where the authors still rely on the DDPM equations.

To the best of our knowledge, we are the first to directly model this problem using SDE, which captures the dynamics of the noise process, and derive the sampling equation which is then used to perform denoising.

## 3. Methods

### 3.1. SDE and Diffusion models

In this section, we give a brief overview of Stochastic Differential Equations, Itô's calculus, and the application to generative modelling.

Let  $\beta(t)$  be a Brownian motion indexed by time  $t$ , i.e.  $\beta(t)$  is a random process with independent and zero-mean Gaussian increment, then the classic result from Itô's calculus gives

$$\int \beta(t)d\beta(t) = \frac{1}{2}\beta^2(t) - \frac{1}{2}t \quad (1)$$

or in a more compact differential form

$$\frac{1}{2}d\beta^2(t) = \beta(t)d\beta(t) + \frac{1}{2}dt \quad (2)$$

This seminal result plays a central role in solving SDE, whose informal definition can be given by the following differential equation

$$dx(t) = f(x(t), t)dt + L(x(t), t)d\beta(t) \quad (3)$$

where  $f(\cdot)$ ,  $L(\cdot)$  are some functions,  $x(t)$  is the random process of interest, and  $dx(t)$  represents the (random) infinitesimal change of  $x(t)$ . The remarkable thing about (3) is that, under some smoothness assumptions of  $f(\cdot)$  and  $L(\cdot)$ , there exists a unique SDE that models the reverse process [27]:

$$\begin{aligned} dx(T-t) = & -f(x(T-t), T-t)dt \\ & + L(x(T-t), T-t)d\beta(T-t) \\ & + L^2(T-t)\nabla \log p_{T-t}dt \end{aligned} \quad (4)$$

where  $p_{T-t}$  denotes the distribution of  $x(T-t)$ . This result comes directly from the application of the Fokker-Planck equation, and is sometimes referred to as Anderson's theorem. The extension of these results to multivariate process is straightforward, and detailed proofs can be found in [28][27][29].

A crucial observation is that, if  $\nabla \log p_{T-t}$  is known, then one can run equation (4) to generate new sample  $x(T-t)$  that comes from data distribution  $p_{T-t}(x)$ . This motivates the search for an efficient method to estimate  $\nabla \log p_{T-t}$ , also known as the score function. Let us now denote the estimation of  $\nabla \log p(x)$  as  $s_{\theta}(x)$ , some function parameterized by  $\theta$ , then the surprising result from [30] gives

$$\begin{aligned} \mathbb{E}_x \left[ \frac{1}{2} \|\nabla \log p(x) - s_{\theta}(x)\|_2^2 \right] \\ \propto \mathbb{E}_x \left[ \frac{1}{2} \|s_{\theta}(x)\|_2^2 + \text{trace}(\nabla s_{\theta}(x)) \right] \end{aligned} \quad (5)$$

From (5), one can parameterize  $s_{\theta}(x)$  as a neural network and directly optimize using samples of  $x$  without

needing the knowledge of  $\nabla \log p(x)$ . This result, along with Langevin sampling, was used in [31] to train neural networks for images generation tasks that achieve high-quality results. In the follow-up papers [32][31], the authors tweaked the learning procedure to learn  $\nabla \log p_{T-t}(x)$ , instead of  $\nabla \log p(x)$ , this proved to be more stable and easier to implement, while achieving better results at the same time. In these works, the sampling was done using (4), instead of Langevin dynamics. This approach is referred to as Score-based Generative Models (SGMs).

In a parallel development, [33] proposed a similar framework from Markov chain perspective, which is named Diffusion Denoising Probabilistic Models (DDPM). DDPM formulation leads to a much simpler objective function, which is shown to be equivalent to (5) under Gaussian noise assumption [34]. In this paper, we use the SDE-based formulation since it is more flexible, allowing us to directly model the desired underlying dynamics of the noise process.

### 3.2. Noise models

In this section, we introduce multiplicative noise, and show how SDE can be used to model the dynamics of this process.

A real-valued signal  $x \in \mathbb{R}$  is corrupted by multiplicative noise is modeled as

$$\tilde{x} = \epsilon x \quad (6)$$

where  $\epsilon \in \mathbb{R}$  is a random variable, usually modeled as having Gamma or Log-normal distribution [35], and  $\tilde{x}$  is the corrupted version of  $x$ . Here, we extend this noise process to multi-dimensional  $\mathbf{x} \in \mathbb{R}^d$ , with the assumption that this corruption affects each component independently

$$\tilde{\mathbf{x}} = \mathbf{x} \odot \boldsymbol{\epsilon} \quad (7)$$

where  $\boldsymbol{\epsilon} \in \mathbb{R}^d$  and  $\odot$  represents the element-wise multiplication. We now show that (7) can be well modelled by the following SDE

$$d\mathbf{x} = \alpha(t)\mathbf{x}(t) \odot d\boldsymbol{\beta}(t) \quad (8)$$

where  $\alpha(t)$  is some time-varying scalar function and  $\boldsymbol{\beta}(t)$  is a Brownian motion on  $\mathbb{R}^d$ . Indeed, the solution to (8) (details in the Appendix<sup>1</sup>) is given as

$$x_{t,i} = x_{0,i} \exp \left( \int_0^t \frac{1}{2} \alpha^2(\tau) d\tau + \int_0^t \alpha(\tau) d\beta(\tau) \right) \quad (9)$$

$$= x_{0,i} \exp \left( - \int_0^t \frac{1}{2} \alpha^2(\tau) d\tau + \left( \int_0^t \alpha^2(\tau) d\tau \right)^{\frac{1}{2}} n \right) \quad (10)$$

$$n \sim \mathcal{N}(0, 1)$$

<sup>1</sup>Appendix is provided in Supplemental materials

where  $x_{t,i}$  denotes the  $i$ -th entry of  $\mathbf{x}(t)$ . Since  $n$  is Gaussian, the exponential term in (8) will follow Log-normal distribution, satisfying our previous assumption on  $\epsilon$ . If we select  $\mathbf{x}(0)$  to be the clean image  $\mathbf{x}$ , then with appropriate value of  $t$ ,  $\tilde{\mathbf{x}}$  can be well modelled by (8).

We can now apply Anderson's theorem to derive the reverse SDE for (8) and use score-matching method from [36] to construct a denoising model. But this formulation gives a rather complicated reverse SDE, as shown in the Appendix. For this reason, we propose to apply a simple logarithmic transformation to  $\mathbf{x}$ , this yields a much simpler reverse SDE, with the additional advantage of being able to apply the results from [34], making the loss function easier to derive.

### 3.3. Loss function in the logarithmic domain

Let us denote  $y_{t,i} = \log x_{t,i}$ . Now, equation (9) becomes

$$y_{t,i} = y_{0,i} - \int_0^t \frac{1}{2} \alpha^2(\tau) d\tau + \int_0^t \alpha(\tau) d\beta(\tau) \quad (11)$$

which can also be expressed in differential form to obtain the SDE

$$dy_{t,i} = -\frac{1}{2} \alpha^2(t) dt + \alpha(t) d\beta(t) \quad (12)$$

Equation (12) can also be written in vector form

$$d\mathbf{y}_t = -\frac{1}{2} \alpha^2(t) \mathbf{1} dt + \alpha(t) d\boldsymbol{\beta}(t) \quad (13)$$

which has the corresponding reverse SDE (proof in the Appendix)

$$d\mathbf{y}_{T-t} = \left( \frac{1}{2} \alpha^2(T-t) \mathbf{1} + \alpha^2(T-t) \nabla \log p_{T-t}(\mathbf{y}_{T-t}) \right) dt + \alpha(T-t) d\boldsymbol{\beta}(T-t) \quad (14)$$

where  $T$  is the terminal time index, i.e. at which the forward SDE (13) stopped.

Applying Euler-Maruyama discretization to (13) and (14), where  $\alpha(t)$  is selected to be  $\sqrt{\frac{d\sigma(t)}{dt}}$  with  $\sigma(t)$  is some differentiable function having non-negative slope, gives the

following pair of SDEs

$$\begin{aligned} \mathbf{y}_k &= \mathbf{y}_{k-1} - \frac{1}{2}(\sigma(k) - \sigma(k-1))\mathbf{1} \\ &\quad + \sqrt{\sigma(k) - \sigma(k-1)}\mathbf{n}_k \\ &= \mathbf{y}_0 - \frac{1}{2}(\sigma(k) - \sigma(0))\mathbf{1} + \sqrt{\sigma(k) - \sigma(0)}\mathbf{n}_k \end{aligned} \quad (15)$$

$$\begin{aligned} \mathbf{y}_{K-k} &= \mathbf{y}_{K-k+1} \\ &\quad + \frac{1}{2}(\sigma(K-k+1) - \sigma(K-k))\left(\mathbf{1} + \right. \\ &\quad \left. 2\nabla \log p_{K-k+1}(\mathbf{y}_{K-k+1})\right) \\ &\quad + \sqrt{\sigma(K-k+1) - \sigma(K-k)}\mathbf{n}_k \\ \mathbf{n}_k &\sim \mathcal{N}(\mathbf{0}, \mathbf{1}) \end{aligned} \quad (16)$$

To derive the loss function, note that equation (38) has a Gaussian transition kernel  $p(\mathbf{y}_k|\mathbf{y}_{k-1}) = \mathcal{N}(\mathbf{y}_k; \mathbf{y}_{k-1} - \frac{1}{2}(\sigma(k) - \sigma(k-1))\mathbf{1}, \sigma(k) - \sigma(k-1))$ . Thus, results from [34] applies, which states the following connection between SGMs and DDPMs: let  $\mathbf{s}^*(\mathbf{x}_t, t)$  and  $\mathbf{n}^*(\mathbf{x}_t, t)$  be the minimizers of SGM and DDPM objectives, respectively, then  $\mathbf{n}^*(\mathbf{x}_t, t) = -\sqrt{\text{var}(\mathbf{x}_t)}\mathbf{s}^*(\mathbf{x}_t, t)$  if  $p(\mathbf{x}_t|\mathbf{x}_{t-1})$  is Gaussian, where  $\text{var}(\mathbf{x}_t)$  denotes the variance of the stochastic process at time  $t$ . This means the denoising objective from DDPM can be readily applied to our formulation in the logarithmic domain, giving the following trainable loss

$$\mathcal{L}_{\theta, \text{discete}} = \mathbb{E}_{\mathbf{y}} \mathbb{E}_k \left[ \|\mathbf{n}_k + \sqrt{\sigma(k) - \sigma(0)}\mathbf{s}_{\theta}(\mathbf{y}_k, k)\|_2^2 \right] \quad (17)$$

where the plus sign is due to the score function being opposite in direction to the noise vector. Thus, by transforming the data into the logarithmic domain, we can take advantage of the simplicity of DDPM framework, while still being able to accurately capture our noise model thanks to the flexibility of SDE. Furthermore, since  $\log$  is a bijective transformation for positive variables, we can easily recover our images from the samples generated in logarithmic domain by taking the exponential. The training and sampling procedures are summarized in Algorithms 1 and 2.

### 3.4. Enhancing image quality by deterministic sampling

Since the sampling equation (14) is a stochastic process, given a noisy input, different runs will result in different denoised images, albeit with the same statistics. This might not be desirable in applications where determinism is required. Thus, we now give two deterministic sampling equations specifically for our proposed SDE. Experimentally, we show that samples generated deterministically achieve substantially better Fréchet inception distance

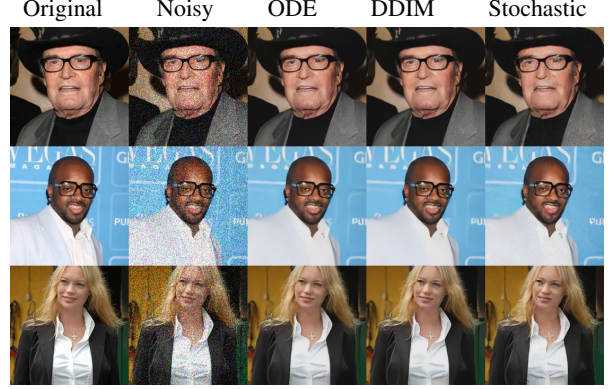


Figure 2. Comparing between different sampling techniques on randomly selected CelebA images, at noise level 0.12. The first two columns include the original images and their noised versions, respectively. These are followed by the results generated by our model using ODE, DDIM, and stochastic samplers, respectively. High resolution version is available in the appendix.

---

#### Algorithm 1 Training procedure of $\mathbf{s}_{\theta}(\mathbf{y}_k, k)$

---

**Input** Training data  $\mathbf{x} \in \mathcal{X}$ , noise schedule  $\sigma(t)$ , number of epochs  $E$ , total steps  $K$

**Output** Score network  $\mathbf{s}_{\theta}(\mathbf{y}_k, k)$ , where  $\mathbf{y} = \log \mathbf{x}$

```

1:  $i = 1$ 
2: while  $i \leq E$  do
3:   for  $\mathbf{x} \in \mathcal{X}$  do
4:      $\mathbf{y} = \log \mathbf{x}$ 
5:     Draw  $k \sim \mathcal{U}(0, K)$ 
6:     Calculate  $\mathbf{y}_k$  according to (38)
7:     Take gradient step on:
        $\mathbb{E}_{\mathbf{y}} \mathbb{E}_k \left[ \|\mathbf{n}_k + \sqrt{\sigma(k) - \sigma(0)}\mathbf{s}_{\theta}(\mathbf{y}_k, k)\|_2^2 \right]$ 
8:   end for
9:    $i = i + 1$ 
10: end while
11: Return  $\mathbf{s}_{\theta}(\mathbf{y}_k, k)$ 

```

---



---

#### Algorithm 2 Noise removal procedure (stochastic)

---

**Input** Corrupted image  $\tilde{\mathbf{x}}$ , number of denoising steps  $K$

**Output** Denoised image  $\hat{\mathbf{x}}$

```

1:  $k = 1, \mathbf{y}_K = \log \tilde{\mathbf{x}}$ 
2: while  $k \leq K$  do
3:    $\nabla \log p_{K-k+1} = \mathbf{s}_{\theta}(\mathbf{y}_{K-k+1}, K - k + 1)$ 
4:   Sample  $\mathbf{y}_{K-k}$  using (16)
5: end while
6: Return denoised image  $\hat{\mathbf{x}} = \exp(\mathbf{y}_0)$ 

```

---

(FID) [37] and Learned Perceptual Image Patch Similarity (LPIPS) [38] metrics

**Probability flows.** Following the idea in [36], from (14), it can be shown that there exists an ODE counterpart whose

marginals match that of (14), this ODE is given as

$$dy_{T-t} = \left( \frac{1}{2}\alpha^2(T-t)\mathbf{1} + \frac{1}{2}\alpha^2(T-t)\nabla \log p_{T-t}(\mathbf{y}_{T-t}) \right) dt \quad (18)$$

which yields the discrete-time equation

$$\begin{aligned} \mathbf{y}_{K-k} &= \mathbf{y}_{K-k+1} \\ &+ \frac{1}{2} \left( \sigma(K-k+1) - \sigma(K-k) \right) \left( \mathbf{1} + \nabla \log p_{K-k+1}(\mathbf{y}_{K-k+1}) \right) \end{aligned} \quad (19)$$

**Implicit probabilistic models.** From the works of [39] [32], given a stochastic process with Markov transition kernel  $p(\mathbf{z}_{t-1}|\mathbf{z}_t)$ , one can design another process with non-Markov transition kernel  $q(\mathbf{z}_{t-1}|\mathbf{z}_t, \mathbf{z}_0)$  whose marginals match, i.e  $q(\mathbf{z}_{t-1}|\mathbf{z}_t) = p(\mathbf{z}_{t-1}|\mathbf{z}_t)$ . For our discretized SDE in (38), its non-Markov counterpart is given as (derivations can be found in Appendix)

$$q(\mathbf{y}_{k-1}|\mathbf{y}_k, \mathbf{y}_0) = \mathcal{N}(\boldsymbol{\mu}_k, \boldsymbol{\Sigma}_k) \quad (20)$$

$$\begin{aligned} \boldsymbol{\mu}_k &= \mathbf{y}_0 - \frac{1}{2}\eta(k-1)\mathbf{1} \\ &+ \frac{\sqrt{\eta(k-1) - \zeta_k^2}}{\sqrt{\eta(k)}} (\mathbf{y}_k - \mathbf{y}_0 + \frac{1}{2}\eta(k)\mathbf{1}) \end{aligned} \quad (21)$$

$$\boldsymbol{\Sigma}_k = \zeta_k^2 \mathbf{I} \quad (22)$$

where  $\zeta_k^2$  is a new parameter controlling the variance of the process, and  $\eta(k) = \sigma(k) - \sigma(0)$ . For deterministic sampling, we can set  $\zeta_k^2 = 0$  and obtain the sampling equations

$$\begin{aligned} \mathbf{y}_{k-1} &= \hat{\mathbf{y}}_0 - \frac{1}{2}\eta(k-1)\mathbf{1} \\ &+ \frac{\sqrt{\eta(k-1)}}{\sqrt{\eta(k)}} (\mathbf{y}_k - \hat{\mathbf{y}}_0 + \frac{1}{2}\eta(k)\mathbf{1}) \end{aligned} \quad (23)$$

and  $\hat{\mathbf{y}}_0$  is given as

$$\hat{\mathbf{y}}_0 = \mathbf{y}_k + \frac{1}{2}\eta(k)\mathbf{1} + \eta(k)\mathbf{s}_\theta(\mathbf{y}_k, k) \quad (24)$$

where  $\mathbf{s}_\theta(\mathbf{y}_k, k)$  is the output of the neural network defined by the objective (17). Equation (24) can be thought of as the best possible prediction of  $\mathbf{y}_0$  in single-step using  $\mathbf{y}_k$ . We note that this approach defines an implicit model that matches the marginals of (38), so the trained  $\mathbf{s}_\theta(\mathbf{y}_k, k)$  can be reused even though we make no use of the original SDE during sampling. This sampler is referred to as Denoising Diffusion Implicit Models (DDIMs) in the literature.

Sampling procedure for these two techniques are provided in Algorithm 3 and 4.

---

### Algorithm 3 Noise removal procedure (ODE)

---

**Input** Corrupted image  $\tilde{\mathbf{x}}$ , number of denoising steps  $K$

**Output** Denoised image  $\hat{\mathbf{x}}$

- 1:  $k = 1, \mathbf{y}_K = \log \tilde{\mathbf{x}}$
  - 2: **while**  $k \leq K$  **do**
  - 3:      $\nabla \log p_{K-k+1} = \mathbf{s}_\theta(\mathbf{y}_{K-k+1}, K - k + 1)$
  - 4:     Compute  $\mathbf{y}_{K-k}$  using (19)
  - 5:      $k = k + 1$
  - 6: **end while**
  - 7: Return denoised image  $\hat{\mathbf{x}} = \exp(\mathbf{y}_0)$
- 

---

### Algorithm 4 Noise removal procedure (DDIM)

---

**Input** Corrupted image  $\tilde{\mathbf{x}}$ , number of denoising steps  $K$

**Output** Denoised image  $\hat{\mathbf{x}}$

- 1:  $k = K, \mathbf{y}_K = \log \tilde{\mathbf{x}}$
  - 2: **while**  $k \leq K$  **do**
  - 3:     Calculate
  - 4:      $\nabla \log p_k = \mathbf{s}_\theta(\mathbf{y}_k, k)$
  - 5:     Compute  $\hat{\mathbf{y}}_0$  using (24)
  - 6:     Compute  $\mathbf{y}_{k-1}$  using (23)
  - 7:      $k = k - 1$
  - 8: **end while**
  - 9: Return denoised image  $\hat{\mathbf{x}} = \exp(\mathbf{y}_0)$
- 

## 4. Experiments

### 4.1. Experiment settings

We ran our experiments on CelebA [40] and UC Merced Land Use [41] datasets, using U-Net [42] as the backbone architecture for our neural networks. The training was done on 100,000 images from the CelebA dataset, while testing was performed on 2,096 images from CelebA holdout set and another 2,096 images from UC Merced Land Use, images were resized to 224x224 pixels. We did not finetune on the land use dataset since we wanted to test the generalization of directly modeling the noise dynamics.

For baseline models, we have selected several denoising methods, ranging from classical signal processing techniques to modern CNN-based frameworks:

- The block-matching and 3D filtering (BM3D) was proposed in [10], it partitions the image into multiple smaller patches and performs collaborative filtering to remove the noise. The method takes advantage of redundancy and consistent information across patches to generate a clean image, it achieved state-of-the-art performance at the times without requiring prior knowledge about noise statistics.
- Speckle reducing anisotropic diffusion (SRAD), proposed in [6], is a method specifically designed for despeckling or multiplicative noise removal. It assumes a set of partial differential equations modeling the noise

Sampling technique	FID ↓	LPIPS ↓	PSNR ↑	SSIM ↑
ODE	<b>13.9156</b>	<b>0.0365</b>	<b>31.8902</b>	<b>0.9348</b>
DDIM	25.3188	0.0882	28.6549	0.9032
Stochastic	32.3811	0.1075	26.8267	0.8493

Table 1. Comparison of different sampling techniques on CelebA dataset at noise level 0.12

Dataset		CelebA				UC Merced Landuse			
Noise level	Model	FID ↓	LPIPS ↓	PSNR ↑	SSIM ↑	FID ↓	LPIPS ↓	PSNR ↑	SSIM ↑
0.04	Ours (ODE)	<b>13.9156</b>	<b>0.0365</b>	31.8902	0.9348	<b>35.7451</b>	<b>0.0753</b>	31.2300	0.9137
	DeblurGAN	18.7211	0.0545	29.6118	0.9274	50.6455	0.1291	29.7493	0.8971
	Restormer	21.9359	0.0523	<b>34.1125</b>	<b>0.9664</b>	51.3572	0.1043	<b>32.7498</b>	<b>0.9377</b>
	MPRNet	23.0067	0.0544	34.0028	0.9654	64.2903	0.1176	32.5545	0.9352
	NAFNet	20.5896	0.0503	34.0764	0.9661	51.4628	0.1063	32.4929	0.9322
	DnCNN	26.8650	0.0726	33.1393	0.9542	111.3414	0.1628	31.8040	0.9217
	SRAD	47.7516	0.2374	27.5801	0.8476	70.5202	0.3565	27.7434	0.8318
	CBM3D	25.1978	0.1282	29.5931	0.9067	74.0214	0.2553	29.8244	0.8836
0.08	Ours (ODE)	<b>19.0333</b>	<b>0.0580</b>	29.8902	0.9148	<b>50.6311</b>	<b>0.1067</b>	29.6971	0.8887
	DeblurGAN	30.8884	0.0737	26.0591	0.8690	79.0759	0.1668	27.6491	0.8553
	Restormer	27.5327	0.0728	<b>32.5138</b>	<b>0.9551</b>	67.5050	0.1437	<b>31.1680</b>	<b>0.9162</b>
	MPRNet	29.0643	0.0772	32.3741	0.9534	90.8632	0.1700	30.9350	0.9116
	NAFNet	25.3441	0.0693	32.4876	0.9546	71.6357	0.1403	30.9993	0.9131
	DnCNN	27.7345	0.0834	31.5783	0.9426	126.2552	0.1867	30.2481	0.8978
	SRAD	60.6093	0.3162	25.7904	0.7835	91.9534	0.4235	26.3913	0.7772
	CBM3D	31.2749	0.1774	27.4770	0.8726	89.7331	0.3181	28.1350	0.8433
0.12	Ours (ODE)	<b>24.3077</b>	<b>0.0774</b>	28.5567	0.8994	<b>63.2679</b>	<b>0.1333</b>	28.8183	0.8727
	DeblurGAN	38.3176	0.0902	24.3920	0.8360	93.9357	0.1916	26.1810	0.8218
	Restormer	29.6475	0.0848	<b>31.5912</b>	<b>0.9473</b>	76.1931	0.1653	<b>30.2727</b>	<b>0.9016</b>
	MPRNet	31.5731	0.0906	31.4240	0.9447	98.2022	0.1884	30.0573	0.8965
	NAFNet	27.0304	0.0805	31.5588	0.9466	77.2864	0.1644	30.0889	0.8977
	DnCNN	33.2722	0.1113	30.5007	0.9281	138.2030	0.2361	29.2134	0.8710
	SRAD	70.4303	0.3853	24.3354	0.7311	107.6315	0.4712	25.2329	0.7247
	CBM3D	36.2575	0.2128	26.1749	0.8481	100.1406	0.3570	27.1042	0.8144

Table 2. Comparison of different denoising methods for various metrics at different noise levels on CelebA and UC Merced Landuse dataset. The best performance for each metric is highlighted in bold.

characteristics and iteratively adjusts the value of each pixel based on the local intensity variations.

- In [11], DnCNN was proposed to perform Gaussian denoising in latent space using CNN and residual learning. It popularized the idea of learning the noise (residuals) of a noisy image instead of directly learning the clean version. DnCNN remains an important tool today and is widely available in image processing toolboxes such as Matlab.
- MPRNet [21] and Restormer [22], a family of image restoration models that utilize multiple scales and transformer architecture to perform the inversion. These models are very competitive with NAFNet in terms of PSNR and SSIM, but we found that NAFNet still beats them in perception metrics.
- NAFNet [13], the current state-of-the-art in noise removal and image restoration. It incorporates multiple advances made by DnCNN, HINet [43], SwinIR [44], BasicSR [12] and others. We make comparison with the width-64 ver-

sion of NAFNet, since this model has 116M parameters, which is comparable to ours, which has 108M.

- Finally, since Generative Adversarial Networks (GANs) do optimize for perception metrics, we also make comparison with GAN-based models by adapting DeblurGAN [45] to our dataset.

Regarding training settings, we trained our model with  $T = 500$  diffusion steps, linear noise schedule  $\sigma(k) \in [0.0001, 0.02]$ , and Adam optimizer [46]. For DnCNN<sup>2</sup>, NAFNet<sup>3</sup>, MPRNet<sup>4</sup>, Restormer<sup>5</sup>, and DeblurGAN<sup>6</sup>, we followed the optimal training options recommended by the authors on Github. All models are trained for 100 epochs. Training was done on 2x RTX3090 under Ubuntu using Pytorch framework. Since DnCNN, NAFNet, MPRNet,

<sup>2</sup><https://github.com/cszn/DnCNN>

<sup>3</sup><https://github.com/megvii-research/NAFNet>

<sup>4</sup><https://github.com/swz30/MPRNet>

<sup>5</sup><https://github.com/swz30/Restormer>

<sup>6</sup><https://github.com/KupynOrest/DeblurGAN>

Restormer, and DeblurGAN need to be trained for some specific noise levels, we chose three different noise variances  $[0.04, 0.08, 0.12]$  for the noise term in (9), this corresponds to  $T = 100, 200, 300$  in our diffusion process formulation. We note that, while these models need to be trained for each noise level, our framework only needs to be trained once, then inference can be run at different noise levels since the noise dynamics is already captured by the SDE formulation.

For evaluation metrics, we chose to evaluate on perception-based metrics FID, LPIPS and traditional signal processing metrics PSNR, SSIM. While PSNR and SSIM are important measurements in computer vision, they have been shown to not correlate well with human perception on image restoration tasks [38]. In our experiments, we also observed substantial discrepancies between these two types of metrics, more detailed discussion is provided in the next section.

Our code is provided in the appendix.

## 4.2. Experiment results

**Sampling techniques.** We evaluate our model with three different sampling techniques: stochastic sampling (16), ODE sampling (19), and DDIM sampling (23), on images from CelebA holdout set, generated from noise level 0.12. Results are presented in Table 1. It can be seen that samples generated using ODE technique perform substantially better across all metrics, especially in FID and LPIPS. Compared to stochastic sampling, deterministic samplers are up to 57% better at FID, and 66% better at LPIPS. This results in observable differences in generated samples, as can be seen from the qualitative examples provided in Figure 2.

**Results on CelebA dataset.** Quantitative results are presented in the left half of Table 2. Compared to the state-of-the-art models NAFNet and Restormer, our method shows slightly worse performance in "per-pixel" metrics, while achieving significantly better FID and LPIPS scores, across all tested noise levels. This is also true when comparing to DnCNN and MPRNet. We note that these models were architected to directly optimize PSNR during training, thus they strive to achieve the best fidelity at the cost of diverging from the input distribution. For classical methods, CBM3D (the RGB version of BM3D) performs respectably, sometimes even coming close to DnCNN. In contrast, SRAD falls far behind in all metrics, we suspect this is because the tests were conducted using RGB images, while this method was originally designed for grayscale samples only.

For DeblurGAN, while it performs respectably at low noise level, it gets substantially worse than other methods across all metrics when more noise is present in the images. In either case, our method also beats it decisively. This is expected since GANs are difficult to train optimally, and are often beaten by Diffusion models in quality of gener-

ated samples [47].

These observations can also be seen in Figure 3, where we present denoising results of these models at noise level 0.08. Compared to our method, other techniques suffer from over-smoothing and they usually generate samples that lack high-frequency details. This is the drawback of using PSNR as an optimization objective, where the denoisers have the tendency of collapsing into the mean statistics of the images, creating smoothing effect. In contrast, our proposed model tends to be much better at preserving finer details, such as facial hair and clothes wrinkles.

**Out-of-distribution results on Land Use dataset.** To evaluate the generalization capability of our method, we re-run the previous experiments on the UC Merced Land Use dataset, which is a small dataset (containing 2,096 samples) captured from satellites. Besides being out-of-distribution, we note that this is a much harder dataset to do denoising on, due to the blurriness and color shifting of satellite imaging. We present quantitative results in the right half of Table 2. While there is large degradation in performance across the board, we again see that our method achieves the best FID and LPIPS scores, while being slightly worse in terms of PSNR and SSIM. Surprisingly, DnCNN performs much worse in terms of FID, while remaining competitive in the other metrics. This could be related to the incorrect assumption of the FID calculation, which was recently discussed in [48].

Qualitatively, from Figure 4, it is observed that our method retains finer details of the images. DnCNN, NAFNet, MPRNet, Restormer, and DeblurGAN produce over-smoothed samples, losing details of the ground, while SRAD and BM3D generate images that completely lack high-frequency components.

Overall, we see that our method achieves competitive performance on PSNR and SSIM, while producing more realistic samples that are closer to the true input distribution, as measured by FID and LPIPS metrics. Furthermore, we show empirically that the method can generalize well to out-of-distribution dataset, which could be crucial in applications where data samples are limited. We provide more qualitative examples in the Appendix.

## 5. Conclusion

In conclusion, this paper introduces a novel SDE-based diffusion model for removing multiplicative noise. The work presents the construction of the forward and reverse SDEs that directly captures the dynamics of the noise model. In addition, it also establishes the training objective as well as multiple different sampling equations based on Probability flows and DDIM techniques. The proposed model is compared to classical image processing algorithms, including BM3D and SRAD, as well as the modern CNN-based methods. Extensive experiments on different datasets demon-



Figure 3. Comparing between different denoising models on randomly selected CelebA images, at noise level 0.08. The first two columns include the original images and their noised versions, respectively. These are followed by the results generated by our method and other popular techniques. Last two rows present a zoomed in example.

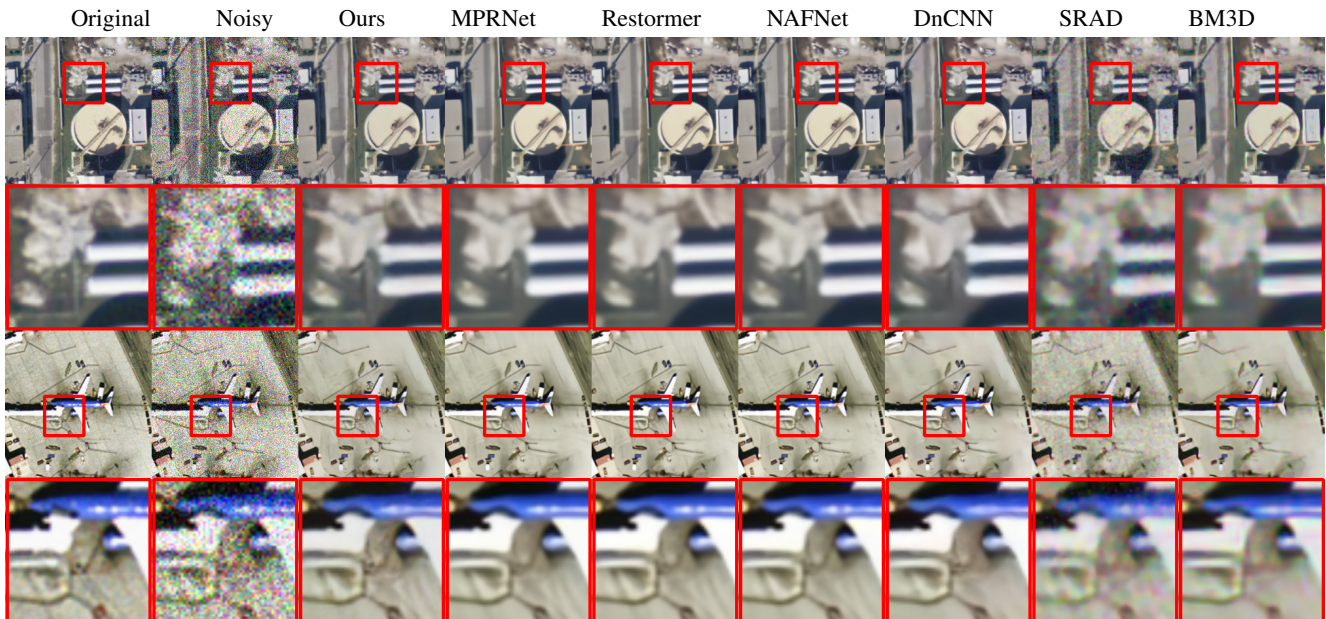


Figure 4. Comparing between different denoising models on randomly selected UC Merced Land Use images, at noise level 0.12. The first two columns include the original images and their noised versions, respectively. These are followed by the results generated by our method and other popular techniques.



strate that our method outperforms the current state-of-the-art denoising models in perception-based metrics across all noise levels, while still remaining competitive in PSNR and SSIM.

Going forward, we will explore the application of diffusion steps reduction techniques to noise removal problems. While these techniques have been applied successfully in generative tasks, it greatly reduces the quality of generated samples in our problem. Thus, care need to be taken when dealing with tasks that are sensitive to small perturbation like denoising. Furthermore, while deterministic sampling is usually used to speedup generation, it is a desirable property in noise removal tasks. Specifically, we would like the process to produce the exact clean image, not something close in terms of distribution, which is modeled by the current diffusion loss. This has connections to conditioning using Doob’s  $h$ -transform, and could hold interesting research venue, we leave it to future works.

## References

- [1] Yu-Mei Huang, Michael K Ng, and You-Wei Wen. A new total variation method for multiplicative noise removal. *SIAM Journal on imaging sciences*, 2(1):20–40, 2009. 1
- [2] José M Bioucas-Dias and Mário AT Figueiredo. Multiplicative noise removal using variable splitting and constrained optimization. *IEEE Transactions on Image Processing*, 19(7):1720–1730, 2010. 1
- [3] Yu-Mei Huang, Lionel Moisan, Michael K Ng, and Tiejong Zeng. Multiplicative noise removal via a learned dictionary. *IEEE Transactions on Image Processing*, 21(11):4534–4543, 2012. 1
- [4] Xiujie Shan, Jiebao Sun, and Zhichang Guo. Multiplicative noise removal based on the smooth diffusion equation. *Journal of Mathematical Imaging and Vision*, 61:763–779, 2019. 1
- [5] Xiangchu Feng and Xiaolong Zhu. Models for multiplicative noise removal. *Handbook of Mathematical Models and Algorithms in Computer Vision and Imaging: Mathematical Imaging and Vision*, pages 1–34, 2021. 1
- [6] Yongjian Yu and Scott T Acton. Speckle reducing anisotropic diffusion. *IEEE Transactions on image processing*, 11(11):1260–1270, 2002. 1, 5
- [7] Bo Chen, Jin-Lin Cai, Wen-Sheng Chen, and Yan Li. A multiplicative noise removal approach based on partial differential equation model. *Mathematical Problems in Engineering*, 2012(1):242043, 2012. 1
- [8] Jianing Shi and Stanley Osher. A nonlinear inverse scale space method for a convex multiplicative noise model. *SIAM Journal on imaging sciences*, 1(3):294–321, 2008. 1
- [9] Gilles Aubert and Jean-Francois Aujol. A variational approach to removing multiplicative noise. *SIAM journal on applied mathematics*, 68(4):925–946, 2008. 1
- [10] Kostadin Dabov, Alessandro Foi, Vladimir Katkovnik, and Karen Egiazarian. Image denoising by sparse 3-d transform-domain collaborative filtering. *IEEE Transactions on image processing*, 16(8):2080–2095, 2007. 1, 5
- [11] Kai Zhang, Wangmeng Zuo, Yunjin Chen, Deyu Meng, and Lei Zhang. Beyond a gaussian denoiser: Residual learning of deep cnn for image denoising. *IEEE Transactions on Image Processing*, 26(7):3142–3155, 2017. 1, 2, 6
- [12] Xintao Wang, Liangbin Xie, Ke Yu, Kelvin C.K. Chan, Chen Change Loy, and Chao Dong. BasicSR: Open source image and video restoration toolbox. <https://github.com/XPixelGroup/BasicSR>, 2022. 1, 6
- [13] Liangyu Chen, Xiaojie Chu, Xiangyu Zhang, and Jian Sun. Simple baselines for image restoration. *arXiv preprint arXiv:2204.04676*, 2022. 1, 2, 6
- [14] Yochai Blau and Tomer Michaeli. The perception-distortion tradeoff. In *Proceedings of the IEEE conference on computer vision and pattern recognition*, pages 6228–6237, 2018. 2
- [15] Dazi Li, Wenjie Yu, Kunfeng Wang, Daozhong Jiang, and Qibing Jin. Speckle noise removal based on structural convolutional neural networks with feature fusion for medical image. *Signal Processing: Image Communication*, 99:116500, 2021. 2
- [16] Hyunho Choi and Jechang Jeong. Speckle noise reduction in ultrasound images using srad and guided filter. In *2018 International Workshop on Advanced Image Technology (IWAIT)*, pages 1–4. IEEE, 2018. 2
- [17] Danlei Feng, Weichen Wu, Hongfeng Li, and Quanzheng Li. Speckle noise removal in ultrasound images using a deep convolutional neural network and a specially designed loss function. In *Multiscale Multimodal Medical Imaging: First International Workshop, MMMI 2019, Held in Conjunction with MICCAI 2019, Shenzhen, China, October 13, 2019, Proceedings 1*, pages 85–92. Springer, 2020. 2
- [18] Tongda Yang, Weiming Wang, Gary Cheng, Mingqiang Wei, Haoran Xie, and Fu Lee Wang. Fddl-net: frequency domain decomposition learning for speckle reduction in ultrasound images. *Multimedia Tools and Applications*, 81(29):42769–42781, 2022. 2
- [19] Jing Zhang, Wenguang Li, and Yunsong Li. Sar image despeckling using multiconnection network incorporating wavelet features. *IEEE Geoscience and Remote Sensing Letters*, 17(8):1363–1367, 2019. 2
- [20] Gang Liu, Hongzhaoning Kang, Quan Wang, Yumin Tian, and Bo Wan. Contourlet-cnn for sar image despeckling. *Remote Sensing*, 13(4):764, 2021. 2
- [21] Syed Waqas Zamir, Aditya Arora, Salman Khan, Munawar Hayat, Fahad Shahbaz Khan, Ming-Hsuan Yang, and Ling Shao. Multi-stage progressive image restoration. In *CVPR*, 2021. 2, 6
- [22] Syed Waqas Zamir, Aditya Arora, Salman Khan, Munawar Hayat, Fahad Shahbaz Khan, and Ming-Hsuan Yang. Restormer: Efficient transformer for high-resolution image restoration. In *CVPR*, 2022. 2, 6
- [23] Soumee Guha and Scott T Acton. Sddpm: Speckle denoising diffusion probabilistic models. *arXiv preprint arXiv:2311.10868*, 2023. 2
- [24] Malsha V Perera, Nithin Gopalakrishnan Nair, Wele Gedara Chaminda Bandara, and Vishal M Patel. Sar despeckling using a denoising diffusion probabilistic model. *IEEE Geoscience and Remote Sensing Letters*, 20:1–5, 2023. 2

- [25] Siyao Xiao, Libing Huang, and Shunsheng Zhang. Un-supervised sar despeckling based on diffusion model. In *IGARSS 2023-2023 IEEE International Geoscience and Remote Sensing Symposium*, pages 810–813. IEEE, 2023. 2
- [26] Naama Pearl, Yaron Brodsky, Dana Berman, Assaf Zomet, Alex Rav Acha, Daniel Cohen-Or, and Dani Lischinski. Svr: Spatially-variant noise removal with denoising diffusion. *arXiv preprint arXiv:2306.16052*, 2023. 2
- [27] Bernt Øksendal and Bernt Øksendal. *Stochastic differential equations*. Springer, 2003. 2
- [28] Kiyosi Ito, Kiyosi Itô, Kiyosi Itô, Japon Mathématicien, Kiyosi Itô, and Japan Mathematician. *On stochastic differential equations*. American Mathematical Society New York, 1951. 2
- [29] Simo Särkkä and Arno Solin. *Applied stochastic differential equations*. Cambridge University Press, 2019. 2
- [30] Aapo Hyvärinen and Peter Dayan. Estimation of non-normalized statistical models by score matching. *Journal of Machine Learning Research*, 6(4), 2005. 2
- [31] Yang Song and Stefano Ermon. Generative modeling by estimating gradients of the data distribution. *Advances in neural information processing systems*, 32, 2019. 3
- [32] Jiaming Song, Chenlin Meng, and Stefano Ermon. Denoising diffusion implicit models. *arXiv preprint arXiv:2010.02502*, 2020. 3, 5
- [33] Jonathan Ho, Ajay Jain, and Pieter Abbeel. Denoising diffusion probabilistic models. *Advances in neural information processing systems*, 33:6840–6851, 2020. 3
- [34] Pascal Vincent. A connection between score matching and denoising autoencoders. *Neural computation*, 23(7):1661–1674, 2011. 3, 4
- [35] HH Arsenuault and G April. Properties of speckle integrated with a finite aperture and logarithmically transformed. *JOSA*, 66(11):1160–1163, 1976. 3
- [36] Yang Song, Jascha Sohl-Dickstein, Diederik P Kingma, Abhishek Kumar, Stefano Ermon, and Ben Poole. Score-based generative modeling through stochastic differential equations. *arXiv preprint arXiv:2011.13456*, 2020. 3, 4
- [37] Martin Heusel, Hubert Ramsauer, Thomas Unterthiner, Bernhard Nessler, and Sepp Hochreiter. Gans trained by a two time-scale update rule converge to a local nash equilibrium. *Advances in neural information processing systems*, 30, 2017. 4
- [38] Richard Zhang, Phillip Isola, Alexei A Efros, Eli Shechtman, and Oliver Wang. The unreasonable effectiveness of deep features as a perceptual metric. In *CVPR*, 2018. 4, 7
- [39] Shakir Mohamed and Balaji Lakshminarayanan. Learning in implicit generative models. *arXiv preprint arXiv:1610.03483*, 2016. 5
- [40] Ziwei Liu, Ping Luo, Xiaogang Wang, and Xiaoou Tang. Deep learning face attributes in the wild. In *Proceedings of International Conference on Computer Vision (ICCV)*, 2015. 5
- [41] Yi Yang and Shawn Newsam. Bag-of-visual-words and spatial extensions for land-use classification. In *Proceedings of the 18th SIGSPATIAL international conference on advances in geographic information systems*, pages 270–279, 2010. 5
- [42] Olaf Ronneberger, Philipp Fischer, and Thomas Brox. U-net: Convolutional networks for biomedical image segmentation. In *Medical image computing and computer-assisted intervention—MICCAI 2015: 18th international conference, Munich, Germany, October 5-9, 2015, proceedings, part III 18*, pages 234–241. Springer, 2015. 5
- [43] Liangyu Chen, Xin Lu, Jie Zhang, Xiaojie Chu, and Cheng-peng Chen. Hinet: Half instance normalization network for image restoration. In *Proceedings of the IEEE/CVF Conference on Computer Vision and Pattern Recognition (CVPR) Workshops*, pages 182–192, 2021. 6
- [44] Jingyun Liang, Jiezhong Cao, Guolei Sun, Kai Zhang, Luc Van Gool, and Radu Timofte. Swinir: Image restoration using swin transformer. *arXiv preprint arXiv:2108.10257*, 2021. 6
- [45] Orest Kupyn, Volodymyr Budzan, Mykola Mykhailych, Dmytro Mishkin, and Jiri Matas. Deblurgan: Blind motion deblurring using conditional adversarial networks. *ArXiv e-prints*, 2017. 6
- [46] DP Kingma. Adam: a method for stochastic optimization. *arXiv preprint arXiv:1412.6980*, 2014. 6
- [47] Prafulla Dhariwal and Alexander Nichol. Diffusion models beat gans on image synthesis. *Advances in neural information processing systems*, 34:8780–8794, 2021. 7
- [48] Sadeep Jayasumana, Srikumar Ramalingam, Andreas Veit, Daniel Glasner, Ayan Chakrabarti, and Sanjiv Kumar. Rethinking fid: Towards a better evaluation metric for image generation. In *Proceedings of the IEEE/CVF Conference on Computer Vision and Pattern Recognition*, pages 9307–9315, 2024. 7
- [49] Peter E Kloeden, Eckhard Platen, Peter E Kloeden, and Eckhard Platen. *Stochastic differential equations*. Springer, 1992. 2
- [50] Christopher M Bishop and Nasser M Nasrabadi. *Pattern recognition and machine learning*. Springer, 2006. 3

# Perception-based multiplicative noise removal using SDEs

## Supplementary Material

### A. Solutions to the forward SDE

Consider the 1-dimensional SDE

$$dx = \alpha(t)xd\beta(t) \quad (25)$$

This can be solved by applying Itô's formula to  $\log x$

$$d \log x = \frac{1}{x} dx - \frac{1}{2x^2} (dx)^2 \quad (26)$$

$$= \frac{1}{x} \alpha(t)xd\beta(t) - \frac{1}{2x^2} \alpha^2 x^2 (d\beta(t))^2 \quad (27)$$

$$= \alpha(t)d\beta(t) - \frac{1}{2} \alpha^2(t)dt \quad (28)$$

$$\Rightarrow \log x_t = \log x_0 - \int_0^t \frac{1}{2} \alpha^2(\tau)d\tau + \int_0^t \alpha(\tau)d\beta(\tau) \quad (29)$$

Recalling a well-known lemma

**Lemma 1.** *Let  $f(t)$  be some function that is square-integrable, i.e.  $\int_0^t f^2(s)ds < \infty$ , and  $\beta(t)$  be a some Brownian motion, then*

$$\int_0^t f(s)d\beta \sim \mathcal{N}\left(0, \int_0^t f^2(s)ds\right) \quad (30)$$

*Proof.* Since Riemann's sum of  $\int_0^t f(s)d\beta$  exists if we fix the midpoints, let  $t_k = \frac{k}{2^n}t$ , then

$$\int_0^t f(s)d\beta = \lim_{n \rightarrow \infty} \sum_{k=0}^{2^n-1} f(t_k)(\beta_{t_{k+1}} - \beta_{t_k}) \quad (31)$$

and since increment of Brownian motion follows  $\mathcal{N}(0, \Delta t)$ , where  $\Delta t = 2^{-n}t$ , thus

$$\sum_{k=0}^{2^n-1} f(t_k)(\beta_{t_{k+1}} - \beta_{t_k}) \sim \mathcal{N}\left(0, \sum_{k=0}^{2^n-1} f^2(t_k)2^{-n}t\right) \quad (32)$$

Now we can take the limit

$$\lim_{n \rightarrow \infty} \sum_{k=0}^{2^n-1} f^2(t_k)2^{-n}t = \lim_{n \rightarrow \infty} \sum_{k=0}^{2^n-1} f^2(t_k)\Delta t \quad (33)$$

$$= \int_0^t f^2(s)ds \quad (34)$$

this completes the proof.

Applying this lemma to (29) gives

$$\log x_t = \log x_0 - \int_0^t \frac{1}{2} \alpha^2(\tau)d\tau + \left( \int_0^t \alpha^2(\tau)d\tau \right)^{\frac{1}{2}} n$$

$$n \sim \mathcal{N}(0, 1)$$

Taking exponential of the last equation yields the desired result.

## B. Derivations of the reverse SDEs

### B.1. In pixel domain

For the reverse SDE, we need to use the more general form of Anderson's theorem

$$dx_{T-t} = \left( -f(x, T-t) + \frac{1}{p_{T-t}(x_{T-t})} \nabla L^2(x, T-t) p_{T-t}(x_{T-t}) \right) dt + L(x, T-t) d\beta_{T-t}$$

Which in our case simplifies to

$$\begin{aligned} dx_{T-t} &= \alpha^2(T-t) \frac{1}{p_{T-t}(x_{T-t})} \nabla x_{T-t}^2 p_{T-t}(x_{T-t}) dt + \alpha(T-t) x_{T-t} d\beta_{T-t} \\ &= \alpha^2(T-t) \left( 2x_{T-t} + x_{T-t}^2 \nabla \log p_{T-t}(x_{T-t}) \right) dt + \alpha(T-t) x_{T-t} d\beta_{T-t} \end{aligned} \quad (35)$$

This reverse SDE is more complicated to work with because of the spatial dependency of the noise term. Due to this, in order to achieve the same convergence guarantee as Euler-Maruyama discretization, more sophisticated schemes such as Milstein's correction needs to be employed [49], making the generative process much more involved. This motivates us to use the logarithmic formulation, which is shown next.

### B.2. In logarithmic domain

Recall that if we apply the logarithmic transform  $y = \log x$ , then the forward SDE takes the form

$$dy_t = -\frac{1}{2} \alpha^2(t) dt + \alpha(t) d\beta(t) \quad (36)$$

which is a simple Wiener process. Applying the previously mentioned Anderson's theorem gives

$$\begin{aligned} dy_{T-t} &= \frac{1}{2} \alpha^2(T-t) dt + \alpha^2(T-t) \frac{1}{p_{T-t}(y_{T-t})} \nabla p_{T-t}(y_{T-t}) dt + \alpha(T-t) d\beta_{T-t} \\ &= \left( \frac{1}{2} \alpha^2(T-t) + \alpha^2(T-t) \nabla \log p_{T-t}(y_{T-t}) \right) dt + \alpha(T-t) d\beta_{T-t} \end{aligned} \quad (37)$$

Since the corruption applies to each pixel independently, this can be trivially extended to multivariate case to obtain the result mentioned in the paper.

## C. Derivation of the deterministic sampling equation using Implicit models

Recall the discretized forward equation presented in the main paper

$$\begin{aligned} \mathbf{y}_k &= \mathbf{y}_{k-1} - \frac{1}{2} (\sigma(k) - \sigma(k-1)) \mathbf{1} + \sqrt{\sigma(k) - \sigma(k-1)} \mathbf{n}_k \\ &= \mathbf{y}_0 - \frac{1}{2} (\sigma(k) - \sigma(0)) \mathbf{1} + \sqrt{\sigma(k) - \sigma(0)} \mathbf{n}_k \end{aligned} \quad (38)$$

This has the Gaussian transition kernel

$$p(\mathbf{y}_k | \mathbf{y}_{k-1}) = \mathcal{N} \left( \mathbf{y}_{k-1} - \frac{1}{2} (\sigma(k) - \sigma(k-1)) \mathbf{1}, (\sigma(k) - \sigma(k-1)) \mathbf{I} \right) \quad (39)$$

$$p(\mathbf{y}_k | \mathbf{y}_0) = \mathcal{N} \left( \mathbf{y}_0 - \frac{1}{2} (\sigma(k) - \sigma(0)) \mathbf{1}, (\sigma(k) - \sigma(0)) \mathbf{I} \right) \quad (40)$$

Consider the non-Markovian kernel

$$p(\mathbf{y}_{k-1} | \mathbf{y}_k, \mathbf{y}_0) = \mathcal{N}(\boldsymbol{\mu}_k, \boldsymbol{\Sigma}_k) \quad (41)$$

$$\boldsymbol{\mu}_k = \mathbf{y}_0 - \frac{1}{2} \eta(k-1) \mathbf{1} + \frac{\sqrt{\eta(k-1) - \zeta_k^2}}{\sqrt{\eta(k)}} (\mathbf{y}_k - \mathbf{y}_0 + \frac{1}{2} \eta(k) \mathbf{1}) \quad (42)$$

$$\boldsymbol{\Sigma}_k = \zeta_k^2 \mathbf{I} \quad (43)$$

where  $\zeta_k^2$  is a new parameter controlling the variance of the process, and  $\eta(k) = \sigma(k) - \sigma(0)$ . We now show that  $q(\mathbf{y}_{k-1}|\mathbf{y}_0)$  matches  $p(\mathbf{y}_{k-1}|\mathbf{y}_0)$ . From [50] (2.115),  $q(\mathbf{y}_{k-1}|\mathbf{y}_0)$  is Gaussian  $\mathcal{N}(\boldsymbol{\mu}_{k-1}, \boldsymbol{\Sigma}_{k-1})$ , and has the following forms

$$\begin{aligned}\boldsymbol{\mu}_{k-1} &= \mathbf{y}_0 - \frac{1}{2}\eta(k-1)\mathbf{1} + \frac{\sqrt{\eta(k-1) - \zeta_k^2}}{\sqrt{\eta(k)}}\left(\mathbf{y}_0 - \frac{1}{2}\eta(k)\mathbf{1} - \mathbf{y}_0 + \frac{1}{2}\eta(k)\mathbf{1}\right) \\ &= \mathbf{y}_0 - \frac{1}{2}\eta(k-1)\mathbf{1}\end{aligned}\tag{44}$$

$$\begin{aligned}\boldsymbol{\Sigma}_{k-1} &= \zeta_k^2\mathbf{I} + \left(\frac{\sqrt{\eta(k-1) - \zeta_k^2}}{\sqrt{\eta(k)}}\right)^2\eta(k)\mathbf{I} \\ &= \zeta_k^2\mathbf{I} + (\eta(k-1) - \zeta_k^2)\mathbf{I} \\ &= \eta(k-1)\mathbf{I}\end{aligned}\tag{45}$$

Thus,  $q(\mathbf{y}_{k-1}|\mathbf{y}_0)$  has the Gaussian kernel

$$\begin{aligned}q(\mathbf{y}_{k-1}|\mathbf{y}_0) &= \mathcal{N}(\boldsymbol{\mu}_{k-1}, \boldsymbol{\Sigma}_{k-1}) \\ &= \mathcal{N}\left(\mathbf{y}_0 - \frac{1}{2}\eta(k-1)\mathbf{1}, \eta(k-1)\mathbf{I}\right) \\ &= \mathcal{N}\left(\mathbf{y}_0 - \frac{1}{2}(\sigma(k-1) - \sigma(0))\mathbf{1}, (\sigma(k-1) - \sigma(0))\mathbf{I}\right) \\ &= p(\mathbf{y}_{k-1}|\mathbf{y}_0)\end{aligned}\tag{46}$$

This completes the proof.

## D. Additional experiment results

We provide more qualitative test samples in Figures 5 and 6. In Fig.5, high-frequency components such as hair and facial wrinkles are better preserved by our method. Whereas other methods have a strong tendency to oversmooth thing, and produce samples that are lacking in this regard. Similarly, in Fig.6, our method tends to retain more high-frequency components compared to others. This results in images that, perceptually, are closer to the original ones.



Figure 5. Comparing between different denoising models on randomly selected CelebA images, at noise level 0.12. The first two columns include the original images and their noised versions, respectively. These are followed by the results generated by our method and other popular techniques.

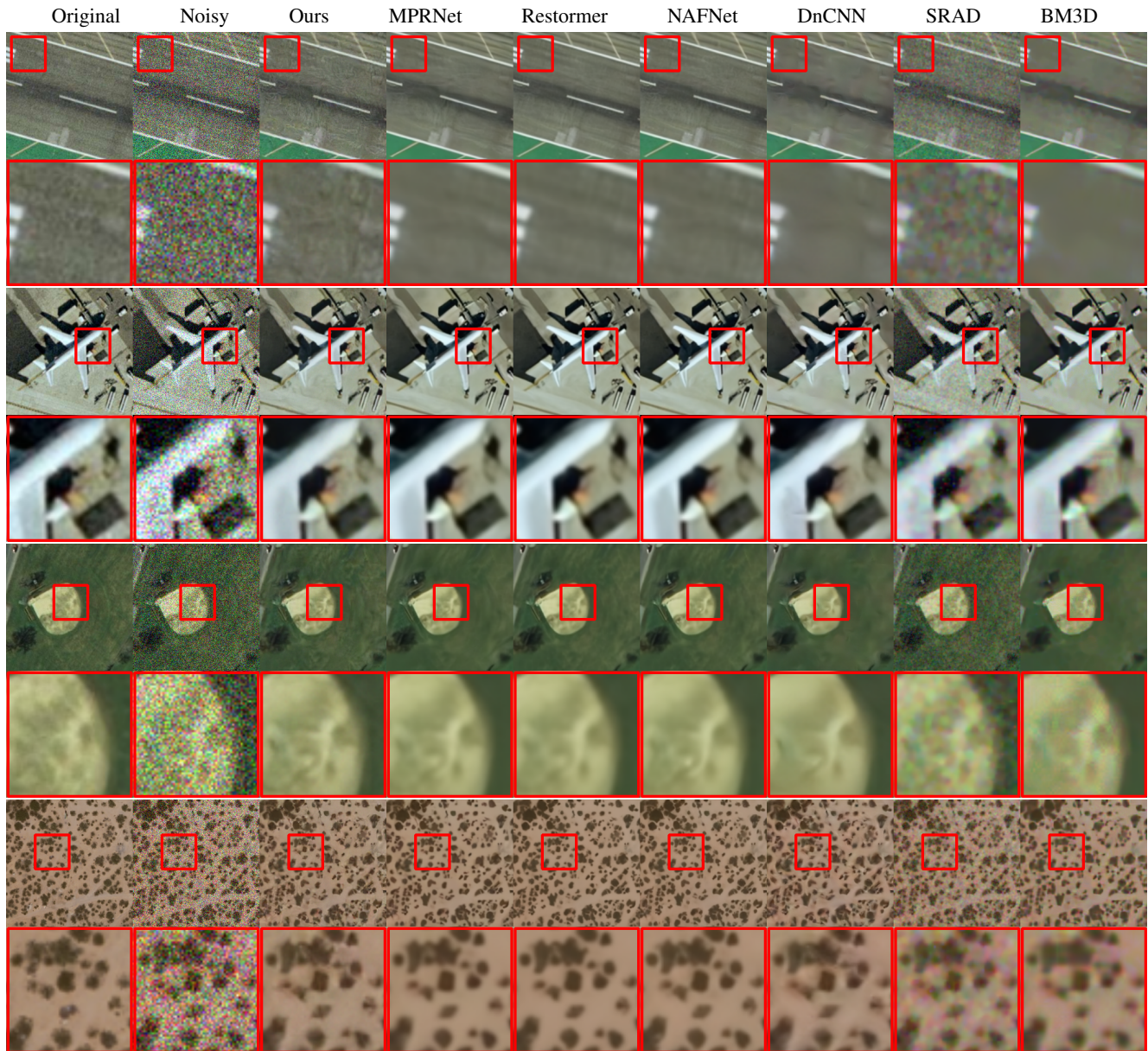


Figure 6. Comparing between different denoising models on randomly selected UC Merced Land Use images, at noise level 0.12. The first two columns include the original images and their noised versions, respectively. These are followed by the results generated by our method and other popular techniques.